Temperature sensitivity of multicrystalline silicon solar cells

Charly Berthod[1], Sissel Tind Kristensen[1], Rune Strandberg[1], Jan Ove Odden[2], Shuai Nie[3], Ziv Hameiri[3], and Tor Oskar Sætre[1]

[1]University of Agder, Grimstad, Norway
[1]REC Solar Norway, Kristiansand, Norway
[3]University of New South Wales, Sydney, NSW, Australia

Abstract **— This paper presents an experimental investigation of the temperature coefficients of multicrystalline silicon solar cells. The aim was to determine if some cell parameters can affect positively the temperature sensitivity without detrimental impact on the efficiency. Commercial solar cells with different bulk resistivities, compensation levels, and cell architectures have been studied. We report that the base net doping, the location of the solar cell along the brick and the cell architecture have significant impacts on the temperature coefficients. Moreover, we show how the change in recombination mechanisms along the ingot height affects the temperature coefficients. The compensation level was observed to have no significant effect on the temperature coefficients. We also demonstrate why aluminum back-surface-field and passivated emitter rear contact solar cells have similar temperature sensitivities despite a better passivation and higher open-circuit voltage for the latter cell architecture. Finally, we have found that reducing the bulk resistivity can improve the solar cells' performance in hot climates.**

D.I. Introduction

Solar cells are normally characterized under standard test conditions (STC), with a temperature of 25 °C, a light intensity of 1000 W/m^2 with an air mass (AM) 1.5G spectrum although solar panels operating in the field very often exceed 25 °C. Temperature increases have a negative effect on solar cell performance [1–3]. In the recent years, more focus has been given to mitigating the losses caused by high temperatures either by using advanced cell architectures [4,5] or by engineering sub-bandgap reflection and radiative cooling [6].

The temperature sensitivity of a solar cell depends on many factors, among them the most well-known element is the open-circuit voltage, V_{oc}. A reduction of the temperature sensitivity can be achieved by increasing the open-circuit voltage, thanks to the use of high-performance cell structures [4,5,7–10]. This means that an efficiency improvement, if caused by an increase of the open-circuit voltage, results in a reduction of the temperature sensitivity. Other factors can also affect the temperature coefficients, such as the base net doping [11–13] the use of an upgraded-metallurgical grade silicon (UMG-Si) as feedstock [11, 14–16], as well as indirect effects such as the wafer position in the brick [17] and light-induced degradation [18].

In this paper, we investigate the possibility of engineering the temperature coefficients. This is done by studying the impacts of the net doping with the compensation level on the temperature sensitivity of multicrystalline silicon (mc-Si) solar cells. First, expressions of the temperature coefficients made by previous authors [1–3, 8] are presented to give an overview of the dependencies with cell parameters [short-circuit current (I_{sc}), open-circuit voltage, fill factor (FF), and efficiency (η)]. Second, experimental temperature coefficients are presented as a function of the cell's position in the brick and of the cell parameters. The brick position of the cells with the lowest temperature sensitivities is investigated. Finally, we show how lowering the resistivity can be a valid method to engineer the temperature coefficients.

D.II. Theoretical Background

The efficiency of a solar cell varies linearly with temperature for the majority of cell types under normal operating temperatures [2]. This variation can be characterized using temperature coefficients. The relative temperature coefficient of a parameter X, β_X, is defined as the rate of change of this parameter over the considered temperature range divided by the value of the parameter at 25 °C

$$\beta_X = \frac{1}{X\,(25^{\circ}\mathrm{C})} \frac{dX(T)}{dT}\bigg|_{T=25^{\circ}\mathrm{C}}. \tag{D.1}$$

The efficiency can be expressed as the product of the open-circuit voltage, the short-circuit current, and the fill factor, divided by the incident solar power. Differentiating this relation and dividing by the efficiency yields

$$\beta_\eta = \beta_{V_{\rm oc}} + \beta_{I\rm sc} + \beta_{FF}. \tag{D.2}$$

The first term is the relative temperature coefficient of the open-circuit voltage ($\beta_{V_{\rm oc}}$) which can be expressed as follows [3]:

$$\beta_{V_{\rm oc}} = \frac{1}{V_{\rm oc}}\frac{dV_{\rm oc}}{dT_{\rm c}} = -\frac{1}{V_{\rm oc}T_{\rm c}}\left[\frac{E_{\rm g0}}{q} - V_{\rm oc} + \gamma\frac{kT_c}{q}\right], \tag{D.3}$$

where $k, q, T_{\rm c}$, and $E_{\rm g0}$ are Boltzmann's constant, the elementary charge, the cell temperature, and the bandgap energy linearly extrapolated to 0 K, respectively. γ is a parameter depending on the limiting recombination mechanisms in the cell and it can be expressed using the external radiative efficiency (ERE) at the open-circuit voltage by [1]

$$\gamma = 1 - \frac{d\ln ERE_{\rm oc}}{d\ln T_{\rm c}} + \left(2\frac{d\ln E_{\rm g}}{d\ln T_{\rm c}} - \frac{d\ln j_{\rm sc}}{d\ln T_{\rm c}}\right), \tag{D.4}$$

where $E_{\rm g}$ is the bandgap energy of the material and $j_{\rm sc}$ the short-circuit current density. ERE is defined as the fraction of the total dark current recombination that is emitted from the cell. γ usually take values from 0 to 5, such as 1.2 in the radiative limit of a crystalline silicon solar cell or 5 for a solar cell limited by Shockley-Read-Hall recombination at the junction (neglecting the temperature dependence of the carrier lifetime and the surface recombination velocity) [19]. The open-circuit voltage decreases with the temperature due to the increase of the dark saturation current, resulting in a negative $\beta_{V_{\rm oc}}$.

The second term of (D.2) is the relative temperature coefficient of the short-circuit current ($\beta_{I\rm sc}$) . The short-circuit current can be written as the product of the ideal short-circuit current ($I_{\rm sc,1sun}$) and the collection fraction ($f_{\rm c}$) . The latter is the fraction of useful photons (with $E \geq E_{\rm g}$) which are collected as carriers in the device. $\beta_{I\rm sc}$ can be expressed as follows [2]

$$\beta_{I\rm sc} = \frac{1}{I_{\rm sc}}\frac{dI_{\rm sc}}{dT_{\rm c}} = \frac{1}{I_{\rm sc,1sun}}\frac{dI_{\rm sc,1sun}}{dE_{\rm g}}\frac{dE_{\rm g}}{dT_{\rm c}} + \frac{1}{f_{\rm c}}\frac{df_{\rm c}}{dT_{\rm c}}. \tag{D.5}$$

This temperature coefficient depends on the variation of $f_{\rm c}$ with temperature, and on the increase of current induced by the bandgap decrease with temperature. Therefore, the coefficient is positive but with a smaller amplitude than $\beta_{V_{\rm oc}}$.

Finally, the last term of (D.2) is the relative temperature coefficient of the fill factor (β_{FF}) . This coefficient can be written as follows [8]

$$\begin{aligned}\beta_{FF} =& \frac{1}{FF}\frac{dFF}{dT_{\rm c}} = (1 - 1.02FF_0)\left(\frac{1}{V_{\rm oc}}\frac{dV_{\rm oc}}{dT_{\rm c}} - \frac{1}{T_{\rm c}}\right) \\ &- \frac{R_{\rm s}}{(V_{\rm oc}/J_{\rm sc} - R_{\rm s})}\left(\frac{1}{R_{\rm s}}\frac{dR_{\rm s}}{dT_{\rm c}}\right),\end{aligned} \tag{D.6}$$

where R_s is the series resistance, FF_0 the ideal fill factor (free of series and shunt resistance effects), and v_{oc} is the normalized open-circuit voltage. The latter two parameters can be expressed as follows:

$$FF_0 = \frac{v_{oc} - \ln(v_{oc} + 0.72)}{v_{oc} - 1} \qquad v_{oc} = \frac{q}{nkT} V_{oc}\,. \tag{D.7}$$

An increase in the open-circuit voltage will increase the FF_0 and reduce the $\beta_{V_{oc}}$ both resulting and in an increase of β_{FF}. The right-hand term in (D.6) is expected to have more variations for cells with large R_s values.

D.III. Experimental Procedure

In this paper, mc-Si solar cells were investigated. Two groups of high-performance G5-ingots were produced, and all wafers were picked from the center brick of these ingots.

The first group of ingots consists of four ingots with the same targeted resistivity and different blend-in-ratios of compensated silicon (made of Elkem Solar Silicon) and non-compensated silicon (material produced by chemical vapor deposition). The wafers were processed into aluminum back surface field (Al-BSF) cells in a laboratory production line. The blend-in-ratio was varied between the ingots to study the effect of compensation level on the temperature coefficients. Ingots with larger blend-in-ratios of Elkem Solar Silicon will see their compensation levels increasing due to a larger addition of compensating dopants. The compensation level can be calculated by dividing the total dopant concentration by the net doping, as shown in the following equation:

$$C_l = \frac{[\mathrm{B}] + [\mathrm{Ga}] + [\mathrm{P}]}{\left([\mathrm{B}^-] + \left[\mathrm{Ga}^-\right]\right) - [\mathrm{P}^+]}. \tag{D.8}$$

The second group of ingots is composed of four ingots with different resistivities ranging from 0.5 to $1.3\,\Omega \cdot \mathrm{cm}$. The ingots were made from the same feedstocks as described previously, one consisting entirely of non-compensated silicon and three of 70 % compensated silicon. Passivated emitter rear contact (PERC) cells were produced in an industrial production line. In this group, the effect of different resistivities on the temperature coefficients is of interest. The initial dopant concentrations and the net doping for these ingots can be found in Table D.1, the data are taken from [20].

The solar cells are standard $15.6 \times 15.6\,\mathrm{cm}^2$ (6 inch) cells, with an approximate thickness of $200\,\mu\mathrm{m}$. The originating wafers were selected at various locations distributed along the height of a center brick of each ingot. All cells underwent a 48 h light-soaking treatment to ensure a degraded state and avoid instabilities during measurements. All values for the distinct ingots are displayed in Table D.2. Note that the average efficiency of Ref is slightly lower than the one for Res 1.3. This is not usually encountered by the

Table D.1: Initial dopant concentrations in the melt, with the net doping averaged between 0 and 90 % of the relative ingot height, for the ingots with different resistivities.

Ingot name	P (cm^{-3})	B (cm^{-3})	Ga (cm^{-3})	Net doping (cm^{-3})
Ref	1.9×10^{16}	5.2×10^{16}	1.6×10^{17}	1.2×10^{16}
Res 0.5	1.9×10^{16}	3.0×10^{16}	1.6×10^{17}	3.8×10^{16}
Res 0.9	1.9×10^{16}	2.4×10^{16}	1.6×10^{17}	1.8×10^{16}
Res 1.3	–	1.3×10^{16}	–	1.2×10^{16}

ingot's producer (REC Solar). Therefore, we suppose it originates from fluctuations in the solidification process from ingot to ingot.

The current-voltage (IV) characteristics of the cells were measured under a standard AM1.5G spectrum with a NeonSee AAA sun simulator. The temperature coefficients of a cell were obtained by measuring the IV characteristics at different temperatures ranging from 25 to 70 °C. The temperature of the measurement chuck was controlled by a water heater. A linear fitting over the temperature range is then performed for each parameter and normalized to 25 °C to obtain the relative temperature coefficient of this parameter.

Note that the values for the open-circuit voltage, the short-circuit current, and the fill factor were normalized with the maximum value of each parameter, and are called "relative" values, so that it is not confused with the normalized open-circuit voltage defined in (D.7).

Sister wafers from ingot CL 4 (see Table D.2) were examined to study the material properties more closely. The wafers were gettered and passivated with silicon nitride (SiN_x) and hydrogenated amorphous silicon (a-Si:H). They were then analyzed using a temperature-dependent photoluminescence (PL) imaging system consisting of an 808 nm diode laser and a silicon charge-coupled device camera. A Sinton WCT-120TS (Sinton Instruments) was integrated into the PL system and was used both to adjust the temperature of the wafer and to calibrate the PL signal into carrier lifetimes. For a more detailed description of the setup and the calibration procedure, see [21]. PL images were acquired at 25 and 70 °C and calibrated into implied V_{oc} at the two temperatures. Maps of $\beta_{iV_{\mathrm{oc}}}$ and γ were then obtained by applying (D.3) at each pixel, following the method in [22].

Table D.2: Description of ingots.

Cell architecture	Ingot name	Targeted resistivity ($\Omega \cdot$ cm)	Dopants	Blend-in ratio (% ESS®)	Efficiency ± STD (%)	V_{oc} ± STD (mV)	I_{sc} ± STD (A)	FF ± STD (%)
Al-BSF	CL1	1.25	B-P	25	16.6 ± 0.2	631 ± 3	8.01 ± 0.05	80.1 ± 0.1
	CL2	1.25	B/Ga-P	40	16.9 ± 0.2	634 ± 3	8.12 ± 0.06	80.1 ± 0.1
	CL3	1.25	B/Ga-P	56	17.0 ± 0.2	634 ± 2	8.14 ± 0.04	79.9 ± 0.1
	CL4	1.25	B/Ga-P	73	16.9 ± 0.1	634 ± 1	8.09 ± 0.02	80.2 ± 0.1
PERC	Ref	1.3	B	0	18.0 ± 0.4	637 ± 8	8.70 ± 0.09	78.9 ± 0.2
	Res 0.5	0.5	B/Ga-P	70	18.2 ± 0.2	650 ± 3	8.57 ± 0.04	79.5 ± 0.2
	Res 0.9	0.9	B/Ga-P	70	18.6 ± 0.3	650 ± 5	8.77 ± 0.07	79.5 ± 0.2
	Res 1.3	1.3	B/Ga-P	70	18.3 ± 0.2	644 ± 3	8.76 ± 0.05	79.1 ± 0.2

D.IV. Results

The four main solar cell parameters vary with the bulk resistivity and the compensation level, which all (including the cell parameters) depend on the position of the cell along the brick. This increases the degree of correlation between these parameters and complicates a correct understanding of the causality. As an example, $\beta_{V_{oc}}$ is improving toward the top of the ingot for Al-BSF cells even though the open-circuit voltage shows a corresponding decrease as shown in a previous study [17]. This result suggests a direct dependency of $\beta_{V_{oc}}$ with the relative height in the brick which needs to be demonstrated. Therefore, in the next section, the temperature coefficients of the four cell parameters will be studied as a function of the cell parameters themselves and the cell's position in the brick.

A. Temperature Coefficient of the Open-Circuit Voltage

In Fig. D.1(a), where $\beta_{V_{oc}}$ is plotted as a function of the relative height in the brick, two distinct trends are observed. The Al-BSF cells (CL 1 to 4) have the highest $\beta_{V_{oc}}$ at the top of the ingot, while the $\beta_{V_{oc}}$ of the PERC cells peak in the middle and decrease near the top. To understand this difference, first the γ parameter will be evaluated. From Fig. D.1(c) we observe that the γ values are decreasing along the whole ingot, except for the PERC cells which flattens out near the top. Nevertheless, the two different architectures show very similar values for γ. This could imply that both types of cells are limited by the same recombination mechanisms. The decreasing trend has a positive effect on $\beta_{V_{oc}}$, i.e., it increases with increasing ingot height. The decrease of $\beta_{V_{oc}}$ for the PERC cells is thus explained by a large decrease of their V_{oc} (not shown here) along the ingot height.

These results are summed up in Fig. D.1(b), where the Al-BSF cells (CL 1 to 4) are found to not follow the V_{oc} trend, instead the data points go perpendicularly as a consequence of the γ variations. The $\beta_{V_{oc}}$ values of the PERC cells are more aligned with the inserted theoretical curve with $\gamma = 2.7$ because of the larger variation of V_{oc} for these cells.

The ingots with different blend-in-ratios vary in compensation levels: starting values at the bottom of the ingot from 1.4 to over 2 for CL 1 and CL 4, respectively (see Fig. D.7 for all values of compensation level). However, these results show that the compensation level does not have any impact on $\beta_{V_{oc}}$ with these levels and this cell architecture. Indeed, the compensation level of the studied cells is mainly below 2.5, which is a relatively low value and higher compensation levels might have an impact. Moreover, the cell architecture, Al-BSF, is not the most sensitive to the material quality and a difference could be observed with more advanced cell architectures such as heterojunction cells. In contrary, the ingots with different resistivities exhibit an advantageous $\beta_{V_{oc}}$ for the cells

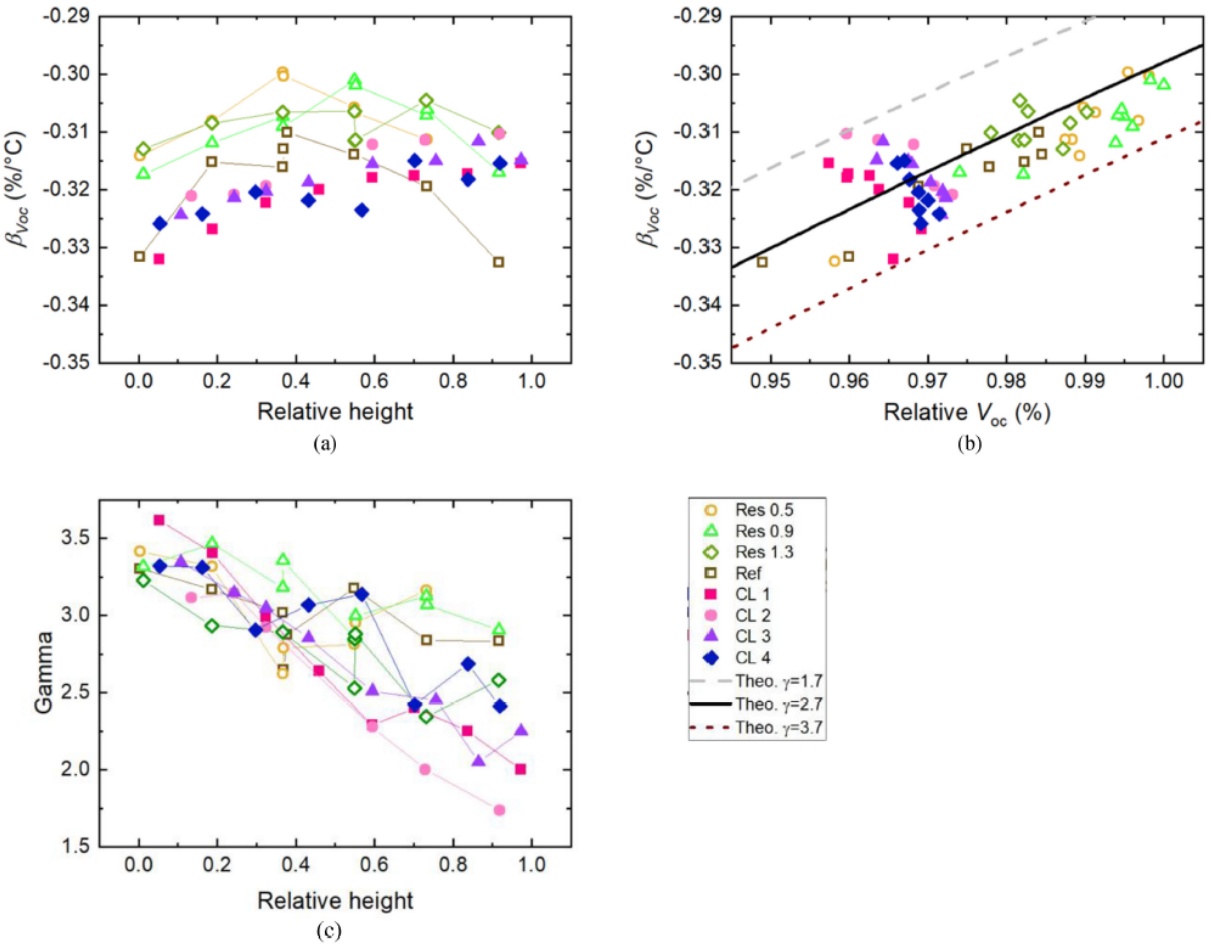

Figure D.1: $\beta_{V_{oc}}$ as a function (a) of the relative height in the brick and (b) of the relative open-circuit voltage with three iso-γ curves, γ-parameter extracted from Eq. (D.3), as a function of (c) the relative height in the brick, for the ingots defined in Table D.2.

made from a low-resistivity material. This is explained by an improvement of V_{oc} [see in Fig. D.1(b)]

To examine what is causing the change in γ values, mapping of this parameter was conducted on sister wafers from ingot CL 4. Fig. D.2 shows the harmonic average of γ over the wafers and the measured γ of the cells as a function of relative brick height. Like the cells, the wafers exhibit a decreasing γ with increasing brick height. However, the wafers display a larger variation along the brick compared to the cells, indicating a variation in limiting recombination mechanism along the brick. The net dopings of the compensated ingots are more constant than the reference ingot [20], we suppose the cause of the variation of γ is a crystallographic defect variation along the ingot.

Figs. D.3(d)-(f) show γ maps of three wafers originating from the bottom, middle, and the top of the brick. The three wafers are highlighted by star symbols in Fig. D.2 for reference. From the maps we observe a relatively uniform and large γ parameter across

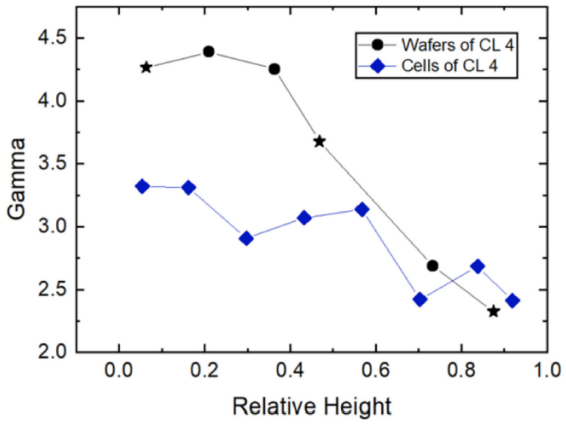

Figure D.2: γ as a function of the relative height in the brick, for wafers and cells in ingot CL 4. The star symbols correspond to the wafers shown in Fig. D.3.

the bottom wafer, whereas the other wafers consist of large areas with low γ values. This is especially the case for the top wafer which consists of large patches with γ values below 2. From corresponding lifetime maps shown on Figs. D.3(a)-(c), the low-γ patches on the top and middle wafers can be identified as areas with high dislocation densities. This suggests that the decrease in γ with brick height observed both for wafers and cells is caused by an increase in dislocation density. These results are corroborated by a recent study that has shown that the temperature coefficient of the lifetime is increasing toward the top of the ingot, due to the increase in low lifetime areas. This causes a decrease of γ [23].

B. Temperature Coefficient of the Short-Circuit Current

In Fig. D.4(a), where $\beta_{I\mathrm{sc}}$ is plotted as a function of the relative height, two different trends are observed for the two different cell architectures. Al-BSF cells (ingots CL 1 to 4) display an increasing $\beta_{I\mathrm{sc}}$ along the ingot height, while no trend is observed for the PERC. The latter has higher I_{sc} values, as can be seen in Fig. D.4(b), as expected for this cell architecture. The two cell types form two quasi-straight lines, suggesting a dependence of $\beta_{I\mathrm{sc}}$ on I_{sc}, as was already observed in previous studies [11, 19]. Two theoretical curves with fixed values for $df_{\mathrm{c}}/dT_{\mathrm{c}}$ are plotted, visualizing the dependence of $\beta_{I\mathrm{sc}}$ with I_{sc} [see (D.5)]. No correlation is observed between the data and the theoretical curves, suggesting that cells with lower I_{sc} values could have larger $df_{\mathrm{c}}/dT_{\mathrm{c}}$, and thus larger $\beta_{I\mathrm{sc}}$.

The four ingots with different compensation levels exhibit different average $\beta_{I\mathrm{sc}}$ values, with the largest found for CL 1. Compensated mc-Si solar cells were shown to possess favorable $\beta_{I\mathrm{sc}}$ values compared to polysilicon cells [14,24,25]. In this paper, the ingot with

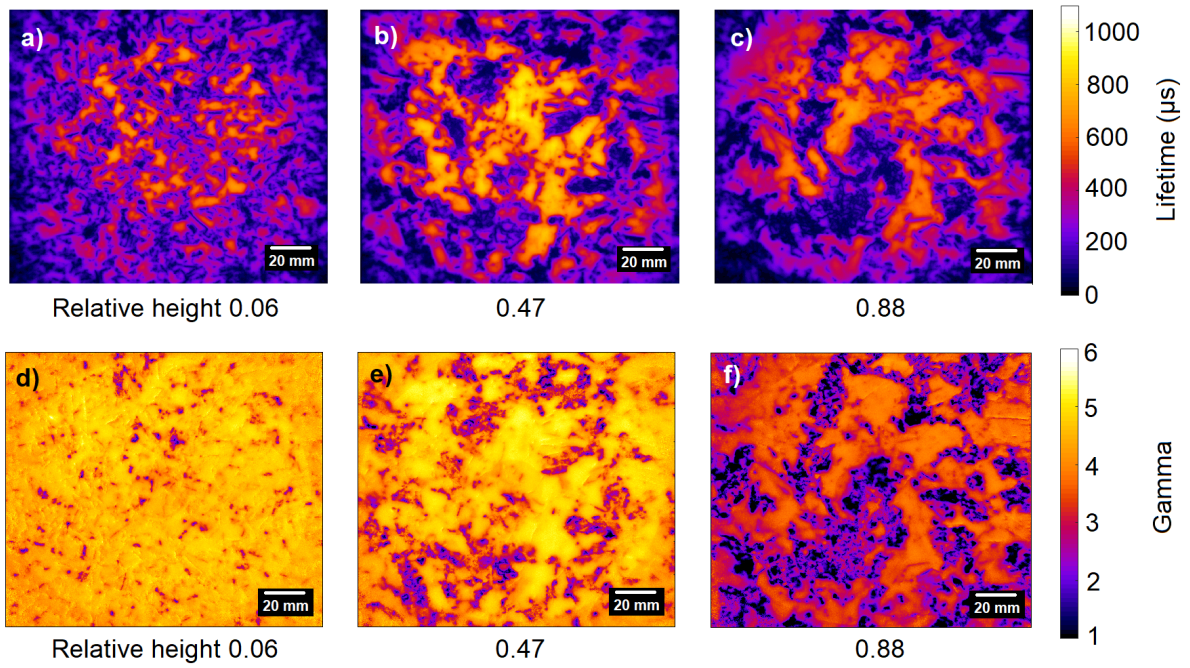

Figure D.3: Lifetime maps at 25 °C (a-c) and γ maps (d-f) of wafers from ingot CL 4 originating from different relative heights in the brick. The maps are obtained from PL imaging and are presented on the same color scale.

the lowest compensation levels (CL 1) shows the best temperature coefficients. Moreover, no distinct trend can be drawn between the different ingots. In conclusion, the compensation level does not have an impact on the temperature coefficients in this case.

The cells from ingot Res 0.5 show the largest β_{Isc} values and consequently (as a result of the sub-mentioned trend) the lowest I_{sc} values. It shows that lowering the bulk resistivity has a negative effect on the I_{sc} which turns out to be beneficial for the temperature coefficient. Several reasons could explain the decrease of I_{sc} such as free carrier absorption, or a less effective back surface field, or even an increased recombination velocity due to higher net doping.

C. Temperature Coefficient of the Fill Factor

The parameter β_{FF} depends heavily on the series resistance, as shown in (D.6). When investigating the dependence of this temperature coefficient with the relative height [see Fig. D.5(a)] we see that the Al-BSF cells with very similar bulk resistivities show very little variations. It is even more pronounced since these cells experienced relatively small variations in V_{oc} and FF, which explains why the data points for these ingots are highly condensed in Fig. D.5(b) and (c), where β_{FF} is plotted as a function of V_{oc} and FF, respectively. In addition, the Al-BSF cells have higher FF and lower V_{oc} values than the

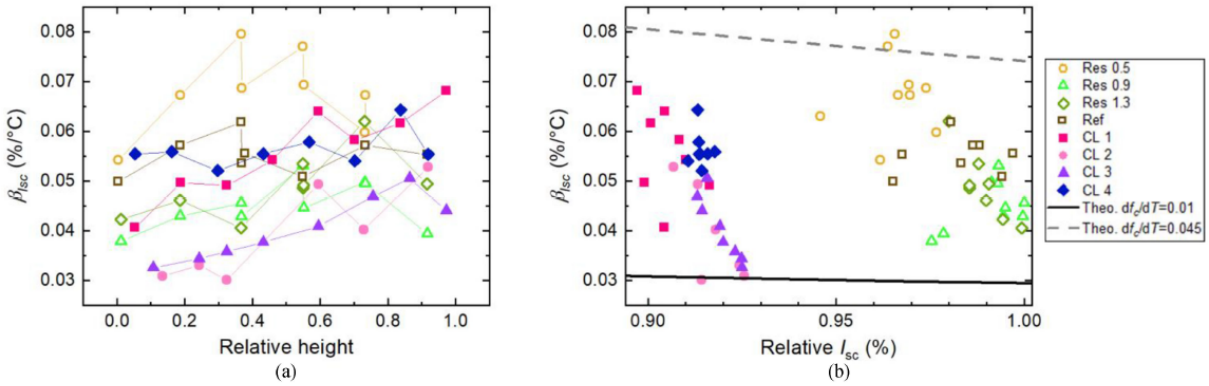

Figure D.4: $\beta_{I_{sc}}$ as a function (a) of the relative height in the brick and (b) of the relative short-circuit current with two iso-df_c/dT_c curves with values of 0.01 and 0.045, for the ingots defined in Table D.2.

PERC cells, which is explained by a reduced series resistance in the cell due to a simpler cell architecture.

On the contrary, the PERC cells show larger variations of V_{oc} and FF between the ingots. An increase of V_{oc} increases $\beta_{V_{oc}}$ and FF_0, thus it increases β_{FF} [see (D.6)]. A lower bulk resistivity positively influences V_{oc}, which increases β_{FF}. Thus, the cells from ingot ESS 0.5 show the largest temperature coefficients, followed by ESS 0.9 and ESS 1.3. The reference ingot Ref exhibits lower values than ESS 1.3 even though the two ingots have similar resistivities. This seems to be the result of a slightly lower V_{oc}.

To study the isolated effect of the resistance on β_{FF}, the parameter φ is introduced, and it is defined as follows:

$$\varphi = \beta_{FF,\mathrm{exp}} - (1.02\, FF_0)\left(\beta_{V_{oc,\mathrm{exp}}} - 1/T_c\right). \tag{D.9}$$

The experimental values of β_{FF} and $\beta_{V_{oc}}$ were used to calculate φ. Meaning the series resistance term in (D.6) is the main part of this parameter, in addition to possible shunt resistance effects, which are not accounted for when calculating β_{FF}. This parameter is plotted against the cells' bulk resistivities in Fig. D.5(d). For the ingots with different resistivities (Res 0.5, 0.9, 1.3 and Ref), φ increases with decreasing bulk resistivity. Moreover, Al-BSF cells with similar bulk resistivities as PERC cells exhibit higher φ values, which is a direct sign of a lower series resistance for this cell architecture. In conclusion, a lower series resistance impacts positively β_{FF}, in accordance with previous results [26].

D. Temperature Coefficient of the Efficiency

The Al-BSF cells least sensitive to temperature variations are situated at the top of the ingot, as can be seen in Fig. D.6. This is explained by a decrease of the γ parameter

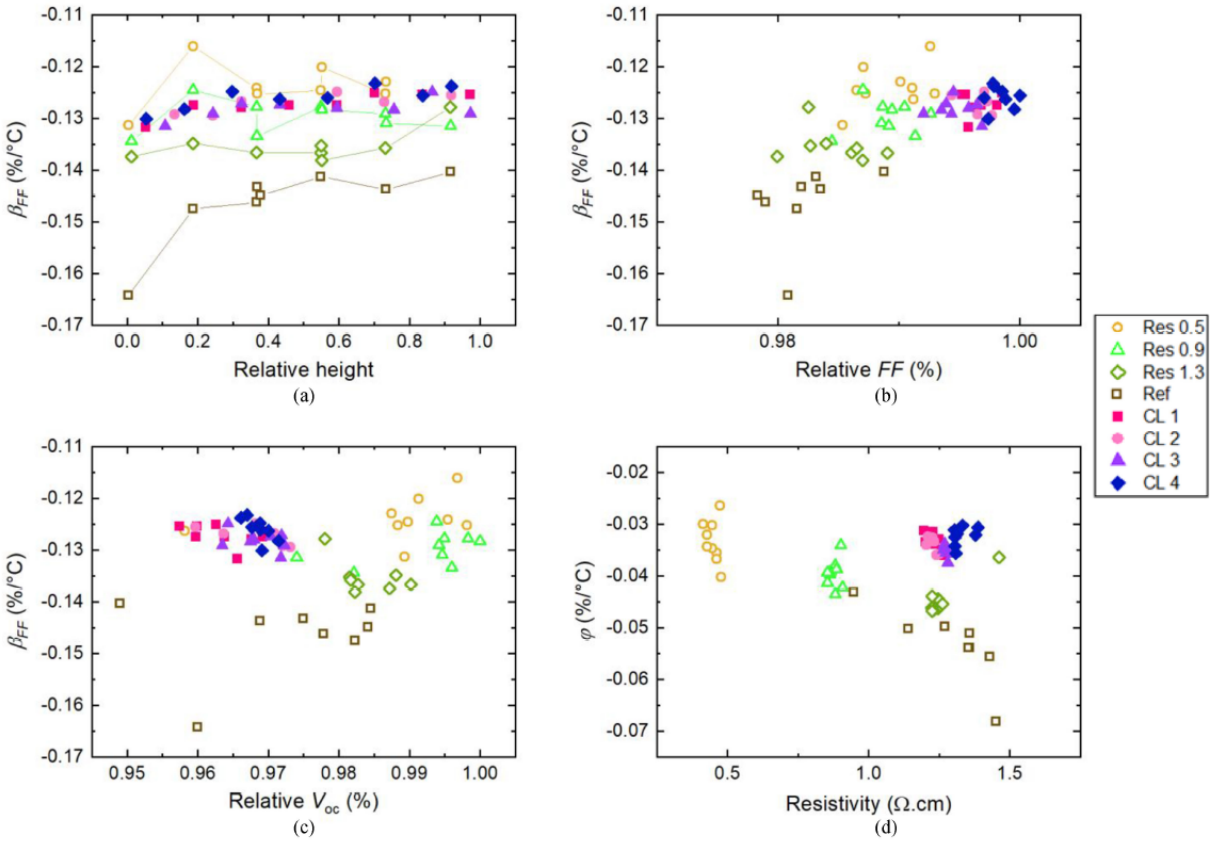

Figure D.5: β_{FF} as a function (a) of the relative height in the brick, (b) of the relative fill factor, and (c) of the relative open-circuit voltage. ϕ, as defined in Eq. D.9, as a function (d) of the bulk resistivity, calculated from the Scheil equation.

along the brick height, increasing $\beta_{V_{\mathrm{oc}}}$, and an increase of $\beta_{I\mathrm{sc}}$. No significant trend can be observed between the different ingots. Ingot CL 4 exhibits higher temperature coefficients for the three bottom cells, but the difference is not significant to draw any conclusion. This is confirmed in Fig. D.7, which shows β_η as a function of the compensation level [defined in (D.8)] for these cells. It can be pointed out that the compensation levels are not particularly high for our material (lower than 2 at the bottom of CL 4), yet these levels are representative of what is obtained when using this compensated feedstock (Elkem Solar Silicon). In addition, these cells have lower efficiencies than state-of-the-art cells. An effect of the compensation level on the temperature coefficient may be observed with high-performance devices.

The PERC cells in Fig. D.6 exhibit the smallest temperature sensitivities around the middle of the brick, due to $\beta_{V_{\mathrm{oc}}}$ which is also at its highest at the same position.

It can be observed that both cell types show relatively similar temperature coefficients even though PERC cells have significantly higher V_{oc} values. Al-BSF cells with lower series resistance experienced an improved β_{FF} which counterbalances the advantageous

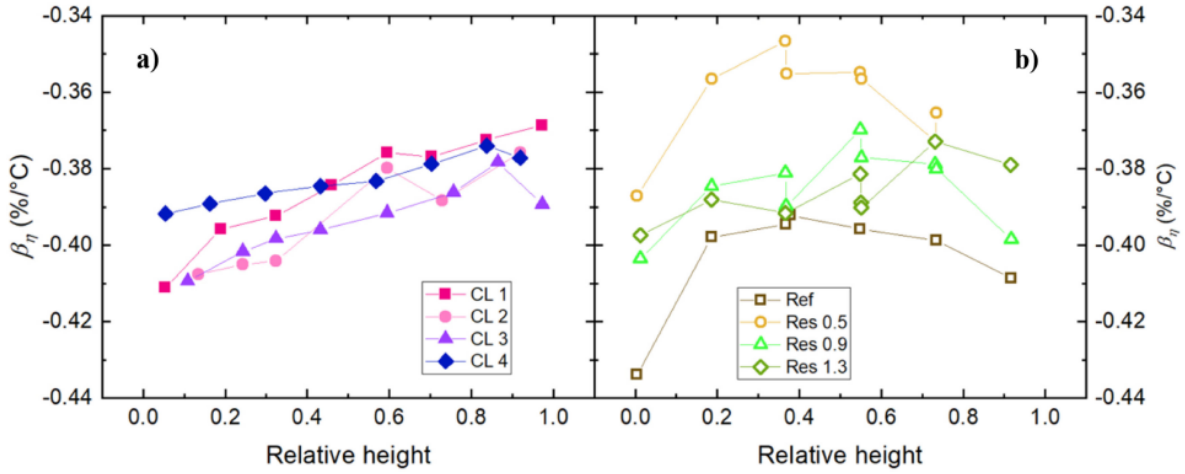

Figure D.6: β_η as a function of the relative height in the brick (a) for the Al-BSF cells and (b) for the PERC cells.

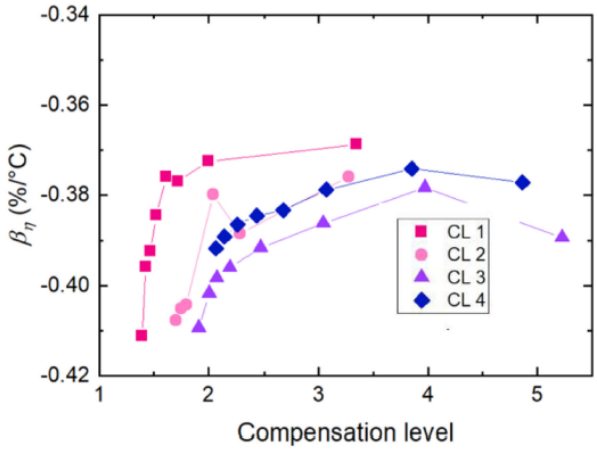

Figure D.7: β_η as a function of the compensation level for the Al-BSF cells.

high V_{oc} and thus $\beta_{V_{\mathrm{oc}}}$ of the PERC cells.

Ingot Res 0.5, which has the smallest bulk resistivity, shows the highest temperature coefficients along the whole brick. Advantageous $\beta_{I\mathrm{sc}}$ and β_{FF} values for this ingot explain the final reduced temperature sensitivity for this ingot. However, the average efficiency for this ingot is smaller than for the two other compensated ingots (Res 0.9 and 1.3). To examine if the lower efficiency at STC is counterbalanced by the reduced temperature sensitivity, Fig. D.8 shows the efficiencies at 25 and 70 °C for the cells in Res 0.5 and Res 1.3. We observe that the mean efficiency of the cells in the low-resistivity ingot is slightly higher than the one for Res 1.3. This means that solar cells made from ingot Res 0.5 will have higher power outputs at high temperatures than cells from Res 1.3. The crossing temperature for the average efficiencies of the two ingots is found to be 45 °C which means that at locations where the operating temperature of modules exceeds

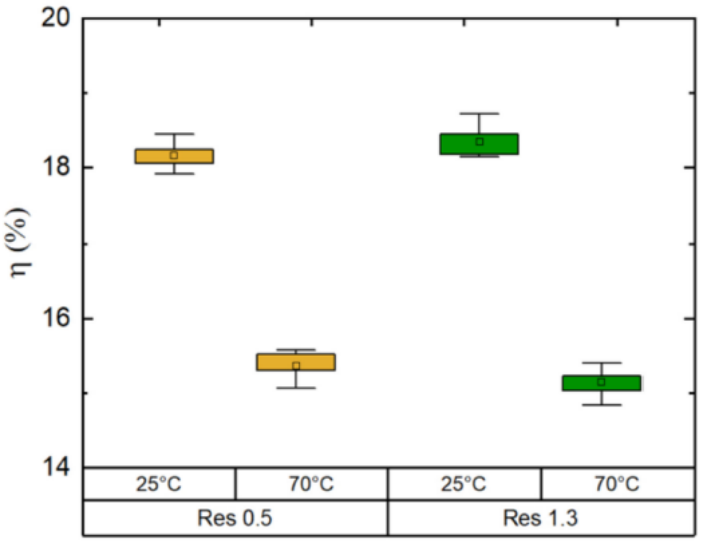

Figure D.8: Box plot of the measured efficiencies of the cells from RES 0.5 and Res 1.3 at STC (25 °C) and 70 °C.

the crossing temperature, the Res 0.5 cells will produce more energy [27]. For the same ingots but a different cell architecture (passivated emitter rear totally diffused cell), the opposite conclusion was reached, which shows the importance of the cell architecture for this technique [28].

D.V. General Discussion

The compensation level is not observed to affect the temperature coefficients at low levels. A problem of many studies is that compensated silicon was obtained by using UMG-Si which has large quality variations between producers. Comparing temperature coefficients of solar cells with large efficiency discrepancies should not be done. In this paper, various blend-in-ratios of an UMG-Si feedstock (Elkem Solar Silicon) were used without changing the efficiency (see Table D.2). This proves the relatively high quality of the used feedstock and enabled us to investigate only the effect of the compensation level without perturbing impurities. Dupré [26] predicted that when UMG-Si would achieve better material and chemical qualities, the gap between the temperature coefficients of solar cells made with this silicon and standard solar cells would vanish. Our study points to the same conclusion.

A previous study tried to engineer solar cells for hot climates by changing the bulk resistivity without success because of a too large drop in efficiency at low resistivities [28]. Here we have successfully managed this method by using PERC cells instead of PERCT cells. This was possible because PERC cells perform better than PERCT cells at low resistivities [29].

D.VI. Conclusion

In this paper, we have shown that dislocation clusters affect positively the temperature coefficient of the open-circuit voltage by decreasing the γ parameter. In addition, we have demonstrated that the compensation level does not influence the temperature sensitivity. Finally, we have shown that decreasing the targeted resistivity of an ingot can be beneficial for the solar cells' performances at high temperatures, depending on the cell architecture.

Acknowledgment

The authors would like to acknowledge the Australian Government through the Australian Renewable Energy Agency (ARENA, Project 2017/RNDO01).

Bibliography

[1] O. Dupré, R . Vaillon, and M. A. Green, "Physics of the temperature coefficients of solar cells," *Sol. Energy Mater. Sol. Cells*, vol. 140, pp. 92-100, 2015.

[2] M. A. Green, "General temperature dependence of solar cell performance and implications for device modelling," *Prog. Photovolt. Res. Appl.*, vol. 11, no. 5, pp. 333-340, 2003.

[3] M. A. Green, *Solar Cells: Operating Principles, Technology and System Applications*. Englewood Cliffs, NJ, USA: Prentice-Hall, 1982, pp. 81-82.

[4] J. Haschke *et al.*, "Nanocrystalline silicon oxide stacks for silicon heterojunction solar cells for hot climates," *AIP Conf. Proc.*, vol. 1999, no. 1, 2018, Art. no. 030001.

[5] J. Haschke *et al.*, "The impact of silicon solar cell architecture and cell interconnection on energy yield in hot & sunny climates," *Energy Environ. Sci.*, vol. 10, no. 5, pp. 1196-1206, 2017.

[6] R. Vaillon, O. Dupré, R. B. Cal, and M. Calaf, "Pathways for mitigating thermal losses in solar photovoltaics," *Sci. Rep.*, vol. 8, no. 1, p. 13163, 2018.

[7] M. Green, K. Emery, and A. Blakers, "Silicon solar cells with reduced temperature sensitivity," *Electron. Lett.*, vol. 18, no. 2, pp. 97-98, 1982.

[8] J. Zhao, A. Wang, S. Robinson, and M. Green, "Reduced temperature coefficients for recent high-performance silicon solar cells," *Prog. Photovolt. Res. Appl.*, vol. 2, no. 3, pp. 221-225, 1994.

[9] T. Mishima, M. Taguchi, H. Sakata, and E. Maruyama, "Development status of high-efficiency HIT solar cells," *Sol. Energy Mater. Sol. Cells*, vol. 95, no. 1, pp. 18-21, 2011.

[10] Y. Lee, C. Park, N. Balaji, Y. J. Lee, and V. A. Dao, "High-efficiency silicon solar cells: A review," *Israel J. Chem.*, vol. 55, no. 10, pp. 1050-1063, 2015.

[11] S. Ponce-Alcántara *et al.*, "A statistical analysis of the temperature coefficients of industrial silicon solar cells," *Energy Procedia*, vol. 55, pp. 578-588, 2014.

[12] M. Mueller, A. Schulze, J. Isemberg, B. Hund, and H. G. Beyer, "Influence of the wafer resistivity on the temperature coefficients of industrial silicon solar cells and on the expected performance behaviour," in *Proc. 25th Eur Photovolt. Sol. Energy Conf. Exhib.*, pp. 2600-2603, 2010.

[13] C. Berthod, R. Strandberg, J. O. Odden, and T. O. Sætre, "Reduced temperature sensitivity of multicrystalline silicon solar cells with low ingot resistivity", in *Proc. IEEE 43rd Photovolt. Spec. Conf.*, pp. 2398-2402, 2016.

[14] F. Tanay, S. Dubois, N. Enjalbert, and J. Veirman, "Low temperature coefficient for solar cells processed from solar-grade silicon purified by metallurgical route," *Prog. Photovolt., Res. Appl.*, vol. 19, no. 8, pp. 966-972, 2011.

[15] M. Tayyib, J. O. Odden, and T. O. Sætre, "Effect of temperature and sun intensity on multicrystalline silicon solar cells," *Proc. 28th Eur. Photovolt. Sol. Energy Conf.*, pp. 1595-1598, 2013.

[16] C. Xiao, X. Yu, D. Yang, and D. Que, "Impact of solar irradiance intensity and temperature on the performance of compensated crystalline silicon solar cells," *Sol. Energy Mater. Sol. Cells*, vol. 128, pp. 427-434, 2014.

[17] C. Berthod, R. Strandberg, and J. O. Odden, "Temperature coefficients of compensated silicon solar cells-influence of ingot position and blend-in-ratio," *Energy Procedia*, vol. 77, pp. 15-20, 2015.

[18] C. Berthod, R. Strandberg, J. O. Odden, and T. O. Sætre, "Reduction of temperature coefficients in multicrystalline silicon solar cells after light induced degradation," in *Proc. IEEE 42nd Photovolt. Spec. Conf.*, pp. 1-5, 2015.

[19] O. Dupré, R. Vaillon, and M. A. Green, "Experimental assessment of temperature coefficient theories for silicon solar cells," *IEEE J. Photovolt.*, vol. 6, no. 1, pp. 56-60, 2016.

[20] R. Søndenå, H. Haug, A. Song, C.-C. Hsueh, and J. O. Odden, "Resistivity profiles in multicrystalline silicon ingots featuring gallium co-doping," *AIP Conf. Proc.*, vol. 1999, no. 1, 2018.

[21] S. T. Kristensen *et al.*, "A high-accuracy calibration method for temperature dependent photoluminescence imaging," in *Proc. SiliconPV*, Leuven, Belgium, 2019.

[22] R. Eberle, S. T. Haag, I. Geisemeyer, M. Padilla, and M. C. Schubert "Temperature coefficient imaging for silicon solar cells," *IEEE J. Photovolt.*, vol. 8, no. 4, pp. 930-936, 2018.

[23] H. Haug, C. Berthod, Å. Skomedal, J. O. Odden, and R. Søndenå, "Simulated and measured temperature coefficients in compensated silicon wafers and solar cells," *Sol. Energy Mater. Sol. Cells*, to be published.

[24] M. Tayyib *et al.*, "Performance assessment of a grid-connected mc-Si PV system made up of silicon material from different manufacturing routes," in *Proc. of IEEE 39th Photovolt. Spec. Conf.*, pp. 0109-0114, 2013.

[25] J. Odden *et al.*, "Results on performance and ageing of solar modules based on elkem solar silicon (ESS) from installations at various locations," *Sol. Energy Mater. Sol. Cells*, vol. 130, pp. 673-678, 2014.

[26] O. Dupré, "Physics of the thermal behavior of photovoltaic devices," Ph.D. dissertation, INSA de Lyon, Villeurbanne, France, 2015.

[27] O. Dupré, R. Vaillon, and M. A. Green, *Thermal Behavior of Photovoltaic Devices: Physics and Engineering*. New York, NY, USA: Springer, 2017.

[28] C. Berthod, S. T. Søndergaard, and J. O. Odden, "Experimental investigation of the optimal ingot resistivity for both the cell performances and the temperature coefficients for different cell architectures," in *Proc. IEEE 7th World Conf. Photovolt. Energy Convers.*, pp. 0293-0297, 2018.

[29] H. Steinkemper, M. Hermle, and S. W. Glunz," Comprehensive simulation study of industrially relevant silicon solar cell architectures for an optimal material parameter choice," *Prog. Photovolt., Res. Appl.*, vol. 24, no. 10, pp. 1319-1331, 2016.